Lessons Learned from Large-Scale Aerospace Structural Testing

Andrew E. Lovejoy[1], Dawn C. Jegley[2], Mark W. Hilburger[3] and Adam Przekop[2]
NASA Langley Research Center, Hampton, VA, 23681, USA

Large-scale testing of aerospace structures is frequently the final step in a development project to validate the structural performance, and that typically involves a large cost and time investment. In order to ensure that the testing provides the required data, avoiding errors that can result in an unsuccessful test and failure to meet objectives is critical. Presented herein are five lessons learned to provide insight to those conducting tests in order to help them avoid known pitfalls that may result in an unsuccessful test. Five subject large-scale tests are described, and include two composite wing tests, a composite hybrid-wing body center section test, a full-scale 27.5-ft diameter metallic barrel test, and an 8-ft diameter metallic barrel test. Problems identified during the testing and mitigation approaches to solve the problems are presented, then the lessons learned are summarized.

I. Introduction

Large-scale testing of representative aerospace structures is used to validate the performance of the structures or to provide full-scale response characteristics for validation of analysis methods. Whenever possible, a building-block approach is commonly used for large-scale testing, where a full-scale test is the culmination of years of research to demonstrate the performance of the final design. In other cases, the full-scale test is used when the proper full-scale response cannot easily be represented by subscale testing, which is particularly true for composite structures where scaled testing is typically not easily accomplished. In either case, these tests represent significant investment in terms of cost and time, and having a successful test is of utmost importance. Lessons learned by researchers at the NASA Langley Research Center (LaRC) from large-scale structural testing conducted at LaRC, NASA Marshall Space Flight Center (MSFC), and NASA Armstrong Flight Research Center (AFRC) are presented in this paper. The test articles examined to provide lessons learned are: the Advanced Composites Technology (ACT) program full-scale 40-ft long semi-span stitched composite wing (SCW) [1]; the Advanced Air Transport Technology (AATT) project 39-ft long, 27% scale tow-steered passive aeroelastic tailored (PAT) wing [2]; the Shell Buckling Knockdown Factor (SBKF) project full-scale 27.5-ft diameter metallic barrels [3]; the SBKF large-scale 8-ft diameter metallic barrels [4]; and the stitched composite Environmentally Responsible Aircraft (ERA) project, 80% scale multi-bay box (MBB) representative of the center section of a hybrid-wing body (HWB) aircraft [5]. Descriptions of the test articles and the testing conducted, descriptions of problems identified during the testing, definitions of developed mitigation approaches to solve the problems, and a summary of the lessons learned are presented in the following sections of this paper.

[1] Research Aerospace Engineer, Structural Mechanics and Concepts Branch, Associate Fellow AIAA.
[2] Senior Research Aerospace Engineer, Structural Mechanics and Concepts Branch, Associate Fellow AIAA.
[3] Principal Technologist for Structures, Materials, and Nanotechnology, Space Technology Mission Directorate, Associate Fellow AIAA.

II. Large-Scale Tests

Lessons learned that will be discussed herein are taken from five large-scale structural tests of aerospace components. Three of the tests are of composite structures, namely the stitched composite wing (SCW) (Section II.A), the passive aeroelastic tailored (PAT) wing (Section II.B), and the multi-bay box (MBB) (Section II.C). The other two tests are large-scale metallic barrel tests, namely the 27.5-ft full-scale (Section II.D) and the 8-ft large-scale tests (Section II.E). Descriptions and details of these tests are presented in the remainder of this section.

A. Stitched Composite Wing

The full-scale 40-ft long SCW was a carbon fiber/epoxy, resin-infused test article with through-the-thickness Kevlar stitches to replace fasteners and suppress damage growth. The SCW consisted of the upper and lower covers, leading and trailing edge spars, and ribs. Figure 1 shows the test setup for the SCW. The test article was attached to the strongback at LaRC using a set of metallic mounting plates that were attached around the perimeter of the test article root region, including the upper and lower covers and the leading and trailing edge spars. The upper and lower covers were of unitized construction with the skin, stringers and intercostals all stitched together. The stitching was applied in all directions in a uniform manner throughout the upper and lower cover skins and the stringers. The leading and trailing edge spars and the ribs were mechanically fastened to the upper and lower covers, and the ribs were also mechanically fastened to the spars. Loads were introduced into the test article using a total of eight hydraulic actuated load lines attached to the test article. These load lines were attached in pairs at four spanwise locations with one actuator at the leading edge (shown in Figure 1) and one actuator at the trailing edge. The pair of actuators at the tip were attached to a metallic closeout rib/fixture, the actuator pair inboard of the tip were attached to a saddle that encapsulated the test article, and the inboard pairs of actuators were attached to local fittings. These eight load lines were used to apply -1g down-bending and 2.5g up-bending load cases. For the third load case, braked roll, an additional line load was added using the load arm shown in Figure 1, which was attached to plates on the upper and lower covers to extend downward behind the wing to simulate a landing gear attachment. A detailed description of the test article, setup and testing is provided in Reference 1.

B. Passive Aeroelastic Tailored Wing

The 39-ft-long, sub-scale tow-steered PAT wing was a carbon fiber/epoxy wing based on a variant of the NASA Common Research Model [6] and included upper and lower skins, leading and trailing edge spars, and 58 ribs [7]. Both skins of the PAT wing were fabricated using tow-steered composites while the spars and ribs were fabricated using conventional composite laminates. Due to numerous manufacturing flaws, including delaminations and wrinkling, a significant repair was made on the leading edge spar where the outboard 11 ft of the composite spar was replaced with an aluminum spar section of nearly equivalent size and performance. Figure 2 shows the PAT wing test set-up at AFRC. The wing was mounted to two root reaction plates that were connected to the leading and trailing edge spars using four 3-in-diameter attachment pins, two in each spar. The root reaction plates were connected to a 6-degree-of-freedom reaction table using angle brackets, with the reaction table supported by load cells at six locations atop a base pedestal. The pedestal was joined to three steel support I-beams that were connected to the load lines, completing a self-reacting test system. Loading was applied using seven pairs of load lines at seven span-wise locations, with one actuator at the leading edge (LE) spar and one at the trailing edge (TE) spar at each spanwise location. Load line pairs were numbered 1 through 7 beginning with location 1 near the root and ending at location 7 at the tip. For the -1g down-bending load condition and the flex axis testing, the load lines were attached to the test article and support I-beams for locations 1 through 6, but at the wing tip (location 7) the load lines were attached to the test article and floor. For the 2.5g up-bending load condition, the outboard three sets of load locations (5, 6, and 7) were connected to the overhead load structure identified in Figure 2, with the steel overhead load structure connected to the support I-beams. The pairs of wing loads at each outboard station were applied using a single loading actuator for each of the load stations, with the three loading actuators embedded in the overhead load structure. Cables connected the loading actuators to the corresponding pairs of wing load connection points at each of the three spanwise loading locations. The cables were guided by movable pulleys that enabled control of the loading direction at each location. The cables were attached to I-beams that split the load to the two wing connection points in a whiffle tree configuration, with the positioning of each overhead cable connection to the whiffle tree I-beams providing the correct load division between the corresponding two wing connection points. A detailed description of the test article, setup and testing is provided in Reference 2.

C. SBKF 27.5-ft-Diameter Metallic Barrels

Two full-scale 27.5-ft-diameter metallic barrel test articles, designated ETTA1 and ETTA2, were each fabricated from eight existing Space Shuttle external tank (ET) panels to support testing at MSFC to update the buckling-critical launch vehicle structure buckling knockdown factors. The ETTA1 and ETTA2 panels were manufactured from Al-Li-2195 flat plate material stock, into which the orthogrid stiffener pattern was machined to form the pockets and weld land details. The flat orthogrid panels were then bump-formed to an Outer Mold Line (OML) radius of 168.0 in. and then heat-treated to their final temper (i.e., the panels were under-formed relative to the final cylinder OML radius of 165.5 in.). Eight curved orthogrid panels were then friction-stir welded together using a vertical weld tool at MSFC to construct a complete 20-ft-tall cylindrical barrel. Figure 3 shows the test setup for the SBKF full-scale testing. The test configuration comprises the load test annex (LTA) crosshead at the top of the setup, hydraulic load lines, an upper load introduction cylinder (ring and simulator), the test article and attachment rings, the lower load introduction cylinder (ring and simulator), and the LTA floor at the bottom of the test setup. The components between the LTA floor and crosshead, termed the stack, included the LH2 load ring through the load lines, and was nearly 70-ft tall. The LTA crosshead and floor constitute rigid boundaries (i.e., ground locations). The upper and lower load introduction cylinders were heritage hardware that were developed for testing the ET intertank, and were designed to represent the stiffness of the liquid oxygen (LO2) tank (upper, or top) and liquid hydrogen (LH2) tank (lower, or bottom), and for which there was limited design information. Test loading consisted of various combinations of axial compression, bending, and internal pressure. Load limits for the test system were 2.25 million pounds of axial compression and 1.4 psi internal pressure, and were limited by the capacity of the hydraulic load actuators used for this setup. A detailed description of the test article, setup and testing is provided in Reference 3.

D. SBKF 8-ft-Diameter Metallic Barrels

As part of the SBKF project, eight large-scale 8-ft-diameter metallic barrels were designed and tested. These sub-scale barrels were designed to have response characteristics similar to large-scale launch vehicle cylindrical structures such as those used in the NASA Space Launch System (SLS) heavy-lift launch vehicle [8]. Orthogrid and isogrid stiffener patterns were used, and each barrel consisted of three Al-Li-2195 panels that were machined flat, then bump formed into the 4-ft radius. The barrels were friction stir welded to form the completed test articles from three panels.

Testing was conducted at MSFC, and Figure 4 shows the test assembly that was designed, analytically verified, and fabricated to meet program test objectives. The test assembly was a self-reacting load system (termed the stack) comprised of an upper and lower load spider, 16 load struts, upper and lower transition sections, the test article assembly, and 8 load lines. Each load line consisted of a hydraulic cylinder, 4-in-diameter loading rod, a load cell, and attachment hardware. The load lines could be controlled independently in load control or stroke (position) control to apply uniform compression or combined compression and bending with a maximum load capability of 1.5 million pounds of axial compression force and 80,000 pounds of axial tension. The test articles were attached to upper and lower load rings using a low-temperature melting point grout and bolts prior to being installed in the stack. During the testing process for the load conditions of axial load, moment load, and combined axial and moment load, the weight of the upper part of the assembly (transition cylinder and spider) was removed from the test article in a tare procedure to remove the weight of the upper load structure so that testing began with zero loads applied to the test article. A detailed description of the test article, setup and testing is provided in Reference 4.

E. Multi-Bay Box (MBB)

The MBB test article was an 80%-scale component representing a section of the most heavily loaded center region of the HWB configuration that was 30-ft long, 14-ft tall, and 7-ft deep. The MBB contained 11 pultruded rod stitched efficient unitized structure (PRSEUS) panels that formed the exterior shell and floor members, along with four interior sandwich rib panels that were used to divide the box width into thirds. In a HWB aircraft, the bulkheads would be near the cockpit and near the tail, while in the test article they are only 7-ft apart. The test article was designed so that these bulkheads would support the same type of loading as would be found in the actual aircraft. Load conditions consisted of mechanical load only that represented -1g down-bending and 2.5g up-bending aerodynamic loads, internal pressure load only, and combined mechanical and internal pressure load. Load introduction boxes were added to the test article to mate with the platens in the Combined Loads Test System (COLTS) facility at LaRC and ensure that the load was introduced into the test article in such a way as to avoid failure at the outer rib locations [5]. Shown in Figure 5 is the test article mounted between the platens in COLTS, having four load lines connecting the platens to apply mechanical loads to the MBB (only two load lines are visible in Fig. 5). Air for internal pressure load was introduced into the bottom section of the MBB. Holes in the floor separating the top and bottom sections permitted the air to equalize pressure throughout the MBB. A detailed description of the test article, setup and testing is presented in Reference 5.

III. Lessons Learned

The five subject large-scale tests presented in the previous section yielded five lessons learned that are associated with test analysis, test design, instrumentation, and load introduction. Lessons are presented herein by first describing the observed response for various tests, and then describing how the data was handled or what measures were taken to mitigate the problem.

A. Lesson 1 – Test Analysis

The first lesson learned is associated with test analysis. Both the SCW and the PAT wing tests had similar challenges that led to an important lesson learned. Often, a test is intended to demonstrate the ability of the structure to satisfy a set of design requirements and sustain the required loads. Tests to demonstrate satisfaction of requirements are designed with the intent that the test applies the actual operational loads, thereby resulting in the correct load distribution within the structure. Applied loading on these two wing test articles was intended to represent specific loads experienced by the wings during service. The SCW test was designed to apply aerodynamic load conditions of -1g down-bending, 2.5g up-bending, and braked roll load conditions, and the PAT wing test was designed to apply aerodynamic load conditions of -1g down-bending and 2.5g up-bending. Preliminary analyses and test design were carried out using linear static analysis for each load condition. However, the deflections of these test articles were large enough that geometric nonlinearity needed to be included in the analysis to accurately capture the test response. Nonlinear static analyses were conducted for both test articles, and the first sets of nonlinear analyses were carried out with the loads applied at the actuator connection points as follower loads because that was more representative of the aerodynamic loads on the real wing. However, as seen in Figures 1 and 2, there were conventional load lines that were connected to the test article at one end and at a fixed point on the other. During testing, the applied test loads remain aligned with the load lines, and were not follower forces with respect to the test article as would be expected for the aerodynamic loads on the real wing.

Failure to initially model the test load conditions accurately resulted in deficiencies with the original test configuration designs. For the SCW, the analyses with applied loads modelled as follower with respect to the test article meant that the loads at the tip remained in the plane of the metallic closeout rib/fixture. As a result, only in-plane forces existed in the metallic rib/fixture. However, as seen in Figure 1 the load lines do not remain coplanar with the closeout rib/fixture. During load application the forces in the test would remain aligned with respect to the load line orientation and not the test article and fixtures, therefore, analyses were updated to keep the load aligned with the load line. Figure 6 shows the finite element model (FEM) with the outboard two sets of load lines and fixtures explicitly modeled. By including beam representations of the load lines and defining the loads as follower loads with respect to those beams, the modified FEM better represented the test condition. This improved FEM accurately captured the test load orientations that resulted in a combination of in-plane and normal forces on the closeout rib/fixture at the tip of the test article. The initial design of this closeout rib/fixture was an unstiffened thick metallic plate. The normal force predicted upon applying the loads consistent with the test configuration resulted in predicted bending stresses sufficient for the metallic closeout rib/fixture to yield. Therefore, as seen in Figures 1 and 6, stiffeners were added to the closeout rib/fixture to alleviate the predicted bending that led to the potential yielding behavior. As a result of the experience with the SCW, similar load lines for the PAT wing were installed at an angle, as shown in Figure 2, so that at the maximum applied test load, the load line would apply load as close to normal to the wing as possible to better represent the aerodynamic loads at maximum load.

Another loading concern that arose in both of the wing tests was response due to eccentric loading. For the SCW, the load arm for the braked roll condition was eccentric from the I-beam extending off the back of the test article. That eccentricity was not included in initial test design analyses. When the eccentricity was included in the analysis model and nonlinear analysis was performed, the load arm was predicted to bend during the test. A mitigation strategy was developed that incorporated an additional load line connected between the strongback and the load arm. The added load line restrained the motion of the load arm adjacent to the braked roll actuator so that the load arm remained nearly in-plane during testing, as initially desired. Figure 7 shows the deflection contours for the load arm where the out-of-plane displacement at the braked roll actuator end was reduced from almost 3.5 in to about 0.2 in, a reduction of displacement of around 95% [Ref. 9]. A similar issue occurred with the PAT wing, where the load lugs to which the load lines were attached were initially modeled with the load applied to the center of the connection pin hole in the plane of the load lug (zero eccentricity). However, the load line was actually connected to one side of the load lug for the test resulting in an eccentric load as shown in Figure 8a. When the eccentricity was included in the final pretest analysis model and nonlinear analysis conducted, excessive bending stresses were predicted that created significant negative margins in several of the lugs. The mitigation was to manufacture couplers so that the load line was attached below the load lug to eliminate the eccentricity and to keep the applied load in the plane of the load lug as shown in Figure 8b. These examples demonstrate the first lesson learned:

Lesson 1) Analyze the test configuration using appropriate analysis approaches.

While tests to assess whether a design satisfies the design requirements are designed with every attempt made to apply loads consistent with how loads are applied to the real structure, that is not always the case. Additionally, details of the fixture design may lead to loads that are eccentric and those eccentricities must be taken into account in the analysis models. Therefore, while analysis of the actual in-service loading scenario is necessary for designing structures, analysis of the actual test setup including the test fixture hardware, eccentricities, and load orientation is necessary to adequately design the test and predict the test response. Lastly, analysis approaches should be appropriate to accurately predict the response, such as using nonlinear analysis when nonlinear response may be present due to large deformations or eccentric loads.

B. Lesson 2 – Load Introduction Structure Response

The second lesson learned is associated with the response of the load introduction structure. The lesson is exemplified by the PAT wing test and the SBKF 8-ft metallic barrel tests that used self-reacting loading structures, and the full-scale 27.5-ft-diameter metallic barrel tests that used heritage hardware. Test analyses typically make assumptions about the boundary conditions and stiffnesses of load introduction structure, often with boundary conditions assumed on the test article and the load introduction structure ignored. The aforementioned tests had load introduction structures that exhibited both rigid-body motions and/or elastic deformation during testing. Because of the possibility of these deformations, digital image correlation (DIC) data and conventional data, including rotations measured with inclinometers or displacement measurements at numerous locations, were collected from the load introduction structure, and that data enabled identification of several load introduction structure responses that led to test and analysis correlation discrepancies. During PAT wing testing the reaction table, pedestal and the structure connecting the reaction table to the pedestal, exhibited both rigid-body motion and elastic deformations. These rigid-body motions and elastic deformations within the self-reacting structure introduced global deflection components that resulted in significant errors in the wing deflection response measurement in the PAT wing testing. By considering the DIC and conventional data collected, rigid body and elastic responses of the load introduction structure could be characterized and used to improve test and analysis correlation by correcting the measured deflection data from the wing. As a result, the test and analysis correlation errors in the wing deflection response were reduced from about 19% to 4% on the inboard portion of the wing when wing motion resulting from the load introduction structure response was subtracted from the measured wing deflections, as shown in Figure 9 [Ref. 10].

In a similar manner, the upper spider and transition cylinder can exhibit rigid-body translations and rotations during the barrel tests. Testing of the 8-ft metallic barrels did identify small rigid-body motions that were not predicted in the high-fidelity FEM, but these motions had little influence on the test article response. Lastly, during the initial full-scale metallic barrel test sequences, the attachment ring region at the intersection of the test article with the load introduction simulators was observed to be rotating about the local tangent direction, which resulted in a poor end shortening test and analysis correlation because axial measurements were taken by displacement transducers attached to these rings. A means of measuring those rotations was implemented that utilized pairs of displacement transducers at each location and enabled adjustment of the axial measurements to improve the end-shortening test and analysis correlation [Ref. 3]. Therefore, the second lesson learned is:

Lesson 2) Characterization of load introduction structure response is critical to understanding test response.

Assumptions about the boundary conditions, including load introduction structure, in an analysis can influence predicted responses, lead to deficiencies in the test design, and lead to poor test and analysis correlation. This is particularly true in self-reacting systems such as those discussed herein that can exhibit rigid-body motion in addition to elastic response, but this can also be seen with test stands that can have “settling” upon the introduction of load as well as deformations of the test stand. Instrumenting load introduction structure can provide data that can enable identification of unexpected load introduction response which can then be used to improve design of the test and improve test and analysis correlation. For test setups that are connected to rigid structure (ground), elastic response of the load introduction structure may occur and should be characterized. Consideration may be particularly important when using heritage hardware and where full details of the hardware design is not available, as was the case for the full-scale metallic barrel tests, which makes accurate modeling of these structures difficult. Therefore, it is also advisable to conduct tests on heritage load introduction structure to characterize its performance whenever possible to help inform modeling of the heritage structure in test modeling.

C. Lesson 3 – Load Application System

The third lesson learned is associated with the applied loads on a test article. In the case of the PAT wing, as mentioned in Section II.A, the inboard pairs of load lines, where the deflections were smaller, were mounted so that the loads at maximum load were applied normal to the wing. However, because of the large wing tip deflections that were expected during the PAT wing up-bending test, an alternate approach was used to apply the three pairs of loads on the outboard part of the wing. For the outer sets of load lines, pairs 5, 6, and 7, AFRC test engineers developed a unique overhead loading structure as shown in Figure 2. The pairs of loads were applied with I-beam spreader bars at each of the three load line locations where in a whiffle tree configuration. The overhead loading assembly included three load actuators to pull the three load cables, combined with three pully position control actuators that changed the position of the cable pullies in the overhead structure (see description in Section I.B). Moving the cable pullies changed the position where the load cables were effectively connected in the overhead structure, thus changing the orientation of the applied load as needed. The ability to move the load cable connection point in the overhead structure allows the load to be applied normal to the wing throughout the loading sequence, and is a very effective approach to control load application orientation and simulate the actual aerodynamic loads on the structure. However, the overhead load structure was designed very early in the project due to scheduling constraints.

When the overhead load structure for the PAT wing test was designed, the predicted displacements were significantly smaller than those eventually observed during the test, and those smaller predicted displacements were used to size the actuator strokes. Also, the motion of the pulley towards the wing root during loading generated additional slack in the line because the distance that the load cable had to traverse from the actuator, over the pulley, and down to the spreader bars was shortened. This shortening of the cable distance created the need for additional stroke of the load application actuator, and this additional stroke was accounted for in the initial design with the initial stroke requirements. Unfortunately, the test article exhibited much larger displacements than expected due to flexibility of the boundary (as described in Lesson 2) and the test article being much more flexible than originally predicted. The larger displacements exhibited by the test article required more pulley motion and, therefore, more pulley and load actuator stroke. However, because the overhead loading fixture was designed and constructed prior to identification of the increased deflections, the additional needed stroke, combined with the geometry of the overhead load structure, led to insufficient stroke in the pulley and load actuators. Therefore, maintaining a normal load orientation throughout loading and at maximum load was not possible. Rather, the load vector rotated from an inboard orientation (acute angle between load vector and upper cover surface inboard of load application point) to an outboard orientation (obtuse angle between load vector and upper cover surface inboard of load application point) as depicted in Figure 10. In the figure, the light blue lines represent the desired orientations with the loads being normal to the wing prior to loading and at the maximum load (and remaining normal throughout loading). To obtain the most normal load at the maximum loads, the pulleys were moved as much as possible within their stroke capabilities and fixed at that location throughout loading. The purple lines depict the orientations of the loads that were set up for the final test with the pulley positions fixed at maximum inward position, and the red lines depict the orientations of the loads at maximum loading with the pulley positions fixed at maximum inward position. Based on this test experience, the third lesson learned is:

> **<u>Lesson 3) Design the load application structure with sufficient margin to account for variability in test article predicted response.</u>**

Whether for conventional load lines on the stitched wing and inboard on the PAT wing, or the moving overhead load application system used outboard on the PAT wing, capability limits of the test setup should not be close to the predicted load and stroke required based on analysis. Rather, significant margin should be applied to the predicted limits of the test article response to ensure that the test setup does not preclude attaining the required test loads and deflections. In the case of the overhead structure, the stroke for the load actuators should have had significant margin to account for possible underestimation of wing deflection and cable slack created by movement of the pulleys. This margin is especially important if the test design is done early in the project, as happened with the PAT wing, and/or with limited information. In cases such as this, an additional margin in stroke capability of 50% would not have been unreasonable and would have permitted sufficient stroke to attain the desired load orientation for the PAT wing test. Similarly, if a buckling test was being developed and then the load capability of the test system should be capable of applying sufficiently large loads in case the buckling load is significantly underpredicted, with the applied margin value being commensurate with the confidence in the predicted value. Thus, additional margins applied to both stroke and load capabilities are recommended, and the amount of margin should be higher for designs finalized earlier in the process and when test article predicted responses are more preliminary in nature, but can be smaller for designs developed closer to the test and when test article responses are better understood.

D. Lesson 4 – Full-Field Response Measurement

The fourth lesson learned is associated with full-field response measurement, and is demonstrated by the MBB testing, where the test article contained thin skins and was subjected to compressive loading. For the MBB structure, buckling was an important consideration. During testing of the MBB, portions of the test article exhibited different response under the same loading condition for different test cycles of that same loading condition. For example, the crown panel on the top of the test article exhibited local buckling of the skins between stiffeners for the up-bending condition that subjected the crown panel to compressive forces. Incorporating as-manufactured imperfections in the analysis has been shown to improve test and analysis correlation, as was seen for the SBKF project. However, as demonstrated by the MBB, even if the imperfections were known and easily incorporated in the predictive analysis, multiple post-buckle equilibria existed for localized responses due to slight variations in testing conditions. As shown in Figure 11, the out-of-plane deformation of the crown panel under the 2.5-g load is dominated by the skin buckling that extends across almost the entire span of the panel. However, as seen in the figure, different buckling patterns were obtained in the pristine and barely visible impact damage (BVID) test load sequences, while the finite element results predicted the same response for pristine and BVID. However, the localized BVID was not applied to the crown panel, and no appreciable effects of the BVIDs were noted elsewhere in the far-field response. Therefore, the uniqueness of the deformation field for structures with multiple stable equilibria in their periodic features cannot be guaranteed, and a particular buckling pattern obtained in each test was likely triggered by otherwise globally insignificant factors such as small manufacturing imperfections, scatter in the applied load path or minor residual stresses from the previous tests and/or servicing of the test article between the tests. Several of the nonlinear finite element analyses were executed with slight changes to solver parameters, for example the integration step increment, and those parameter changes also resulted in nonunique distinct buckling patterns [Ref. 11]. If only a few strain gages were used to monitor the response, the ability to develop a comprehensive understanding of the response might have been compromised. For example, if local skin buckling were to occur during the test in the direction opposite to the pre-test prediction, the comparison of the test and analytical strain data would likely show a qualitatively inaccurate response correlation (tension instead compression or vice versa). This could cause confusion when monitoring response during the test and/or during the post-test data analyses. Therefore, acquiring and monitoring full-field measurements should be incorporated in testing in order to understand response complexities associated with non-unique solutions. Similar necessity for full-field measurements was demonstrated by the examples in Lesson 2 where measurements of the complex boundary response consisting of rigid-body motion and elastic deformation were necessary. Such a capability can be accomplished using DIC as was used for the test results shown in Figure 11 and for the PAT wing boundary characterization of Lesson 2. Therefore, the fourth lesson learned is:

> **<u>Lesson 4) Full-field response measurements are crucial to understanding response when complex, and potentially nonunique, responses may occur.</u>**

Because very small perturbations can result in changes in local buckling patterns, full-field measurements may be necessary to understand the actual local deformation for each loading cycle, particularly for thin-skin or thin-walled structures. The same is true for buckling testing of a structure where there could be multiple global or local buckling modes with identical or very closely spaced eigenvalues. In those cases, the use of a limited number of conventional strain gages may not provide sufficient information to determine the response. Therefore, the use of full-field measurements provides robustness in the test data to account for uncertainties in the response of large-scale, complex structures.

E. Lesson 5 – Residual Stresses

The fifth and final lesson learned presented herein is related to residual stresses and is demonstrated by the full-scale metallic barrel tests. As described in Section I.C, the full-scale barrels were formed by friction-stir welding eight panels that had been formed to 168-in. radius and then heat treated. Prior to welding, the panels were presumed to be in a stress-free state, that is, free from residual stresses due to manufacturing. However, the welding process resulted in local residual stresses at the welds and widespread residual stresses in the full barrel due to bending the panels together, i.e., decreasing their radius, to form the 165.5-in radius of the test article. The residual stresses due to bending of the panels was particularly significant in the circumferential stiffeners, and those residual stresses ranged from small tension in the skin to a compressive maximum at the top edge of the stiffeners as a result of the forming process

[Ref. 3]. Including residual stresses had a small benefit on global response test and analysis correlation. Figure 12 shows the radial displacement contours for the test, the baseline analysis and an analysis including residual stresses. The limits in the contour plots are observed to have much better agreement between the test and the residual stress model results, particularly in the centers of the panels where the circumferential stiffeners have more influence. In fact, the maximum inward (negative) deflection is within 1%, compared to the test and baseline model analysis response that has a difference of over 13%. Additionally, the deflections at the weld lands have improved test and analysis correlation for the outward (positive) displacements where the error between test and the residual stress model analysis are reduced by about a third compared to the error between the test and baseline analysis. Therefore, the fifth lesson learned is:

Lesson 5) Residual stresses can have an effect on test article response, and should be included in the analysis whenever possible.

Understanding the manufacturing process for the test article and considering residual stresses in test articles is important. While it may be difficult to determine the residual stresses in the test article, the residual stresses should be included in analyses to improve test and analysis correlation for test articles that have known residual stresses.

IV. Summary of Lessons Learned

Large-scale testing is an important part of research and development of aerospace structures. Representative aerospace structures tests are used to validate the performance of the structures or to provide full-scale response characteristics without having to test a full-scale structure. However, due to the difficulties that can exist in conducting tests, such as representing correct boundary conditions and applying loads, there are certain lessons learned that need to be considered. Presented herein are five lessons learned from several large-scale tests conducted by researchers at LaRC. Lessons learned were:

- **Analyze the test configuration using appropriate analysis approaches**
- **Characterization of load introduction structure response is critical to understanding test response**
- **Design the load application structure with sufficient margin to account for variability in test article predicted response**
- **Full-field response measurements are crucial to understanding response when complex, and potentially nonunique, responses may occur**
- **Residual stresses can have an effect on test article response, and should be included in the analysis whenever possible**

Researchers and test engineers, from beginner to experienced, should remember these lessons learned when planning and conducting tests and performing test and analysis correlation. While many of these lessons may seem intuitive, they can often be ignored when schedule and cost become crucial aspects of a project if they aren't kept in mind at all times. Application of these lessons have eliminated potential failures of load introduction hardware for the stitched composite wing and the passive aeroelastic tailored wing tests, enabled accurate test and analysis correlation for the PAT wing, the multi-bay box, and the full-scale 27.5-ft and large-scale 8-ft metallic barrels tested, and identified limitations of the overhead load introduction structure for the PAT wing tested. In the end, all of the large-scale tests presented herein were successfully tested due, in part, to understanding and applying these lessons learned. In general, failure to understand and apply these lessons may result in a test that is unable to obtain the desired data or test results, and therefore result in failure to meet project objectives. Engineers should always be on the lookout for uncertainties, the effects of modeling assumptions, and lack of knowledge when designing and analyzing large-scale structural tests.

References

[1] Jegley, D. C., Bush, H G., and Lovejoy, A. E., "Structural Response and Failure of a Full-Scale Stitched Graphite-Epoxy Wing," *Journal of Aircraft*, Vol. 40, No. 6, November-December 2003, pp. 1192-1199.

[2] Jutte, C. V., Wiesemann, C. D., Lovejoy, A. E., and Stafford, B. K., "Static Loads Testing of a High Aspect Ratio Tow-Steered Wingbox," *Proceedings of the 2020 AIAA/ASCE/AHS/ASC Structures, Structural Dynamics, and Materials Conference*, AIAA Paper 2020-0243, Orlando, FL, January 6-10, 2020.

[3] Lovejoy, A. E., Hilburger, M. W and Gardner, N. W., "Test and Analysis of Full-Scale 27.5-Foot-Diameter Stiffened Metallic Launch Vehicle Cylinders," *Proceedings of the 2018 AIAA/ASCE/AHS/ASC Structures, Structural Dynamics, and Materials Conference*, AIAA Paper 2018-1989, Kissimmee, FL, January 8 – 12, 2018.

[4] Hilburger, M. W., Haynie, W. T., Lovejoy, A. E., Roberts, M. G., Norris, J.y P., Waters, W. A., and Herring, H M., "Subscale and Full-Scale Testing of Buckling-Critical Launch Vehicle Shell Structures," *Proceedings of the 53rd AIAA/ASME/ASCE/AHS/ASC Structures, Structural Dynamics and Materials Conference*, AIAA Paper 2012-1688, Honolulu, Hawaii, Apr. 23-26, 2012.

[5] Jegley, D. C., Rouse, M., Przekop, A., and Lovejoy, A. E., "The Behavior of a Stitched Composite Large-Scale Multi-Bay Pressure Box," NASA/TM-2016-218972, April 2016.

[6] Vassberg, J. C., DeHaan, M. A., Rivers, S. M., and Wahls, R. A., "Development of a Common Research Model for Applied CFD Validation Studies," *Proceedings of the 26th AIAA Applied Aerodynamics Conference*, AIAA Paper 2008-6919, Honolulu, Hawaii, August 18 – 21, 2008.

[7] Brooks, T.R., Kenway, G.K.W., Martins, J.R.R.A., "Benchmark Aerostructural Models for the Study of Transonic Aircraft Wings," *AIAA Journal*, Vol. 56, No. 7, pp. 2840-2855, 2018.

[8] Hilburger, M. W., Lovejoy, A. E., Thornburgh, R. P., and Rankin, C., "Design and Analysis of Subscale and Full-Scale Buckling-Critical Cylinders for Launch Vehicle Technology Development," *Proceedings of the 53rd AIAA/ASME/ASCE/AHS/ASC Structures, Structural Dynamics and Materials Conference*, AIAA Paper 2012-1865, Honolulu, Hawaii, Apr. 23-26, 2012.

[9] Lovejoy, A. E., "Finite Element Analysis of a Composite Semi-Span Test Article With and Without Discrete Damage," NASA/CR-2000-210308, August 2000.

[10] Lovejoy, A. E., Gardner, N. W., Dawicke, D. S., Jutte, C. V., and Smith, B., "Improving Structural Test and Analysis Correlation Using Digital Image Correlation Boundary Measurements," *Proceedings of the 2020 AIAA/ASCE/AHS/ASC Structures, Structural Dynamics, and Materials Conference*, AIAA Paper 2020-2188, Orlando, FL, January 6-10, 2020.

[11] Przekop, Adam, Jegley, Dawn C., Lovejoy, Andrew E., Rouse, Marshall, and Wu, Hsi-Yung, "Testing and Analysis of a Composite Non-Cylindrical Aircraft Fuselage Structure, Part I: Ultimate Design Loads," *Proceedings of the 57th AIAA/ASCE/AHS/ASC Structures, Structural Dynamics, and Materials Conference*, AIAA Paper 2016-2176, San Diego, CA, January 4-8, 2016.

[12] Lovejoy, A. E., Hilburger, M. W., Haynie, W. T., Satyanarayana, A., Gardner, N. W., Roberts, M. G., Norris, J. P., and Thornburgh, R. P., "Buckling Analysis and Test Results for Full-scale 27.5-Foot-Diameter Integrally Stiffened Al-Li Cylinder Test Articles," NASA TM (to be published at a later date).

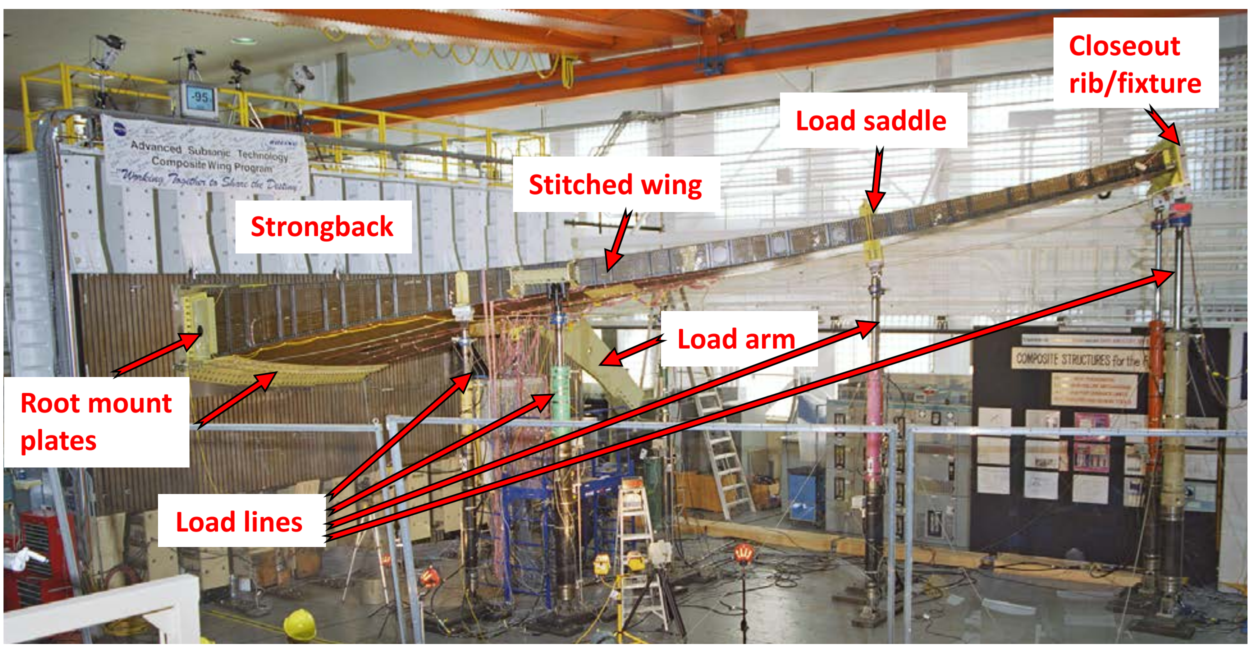

Figure 1. Stitched composite wing test setup.

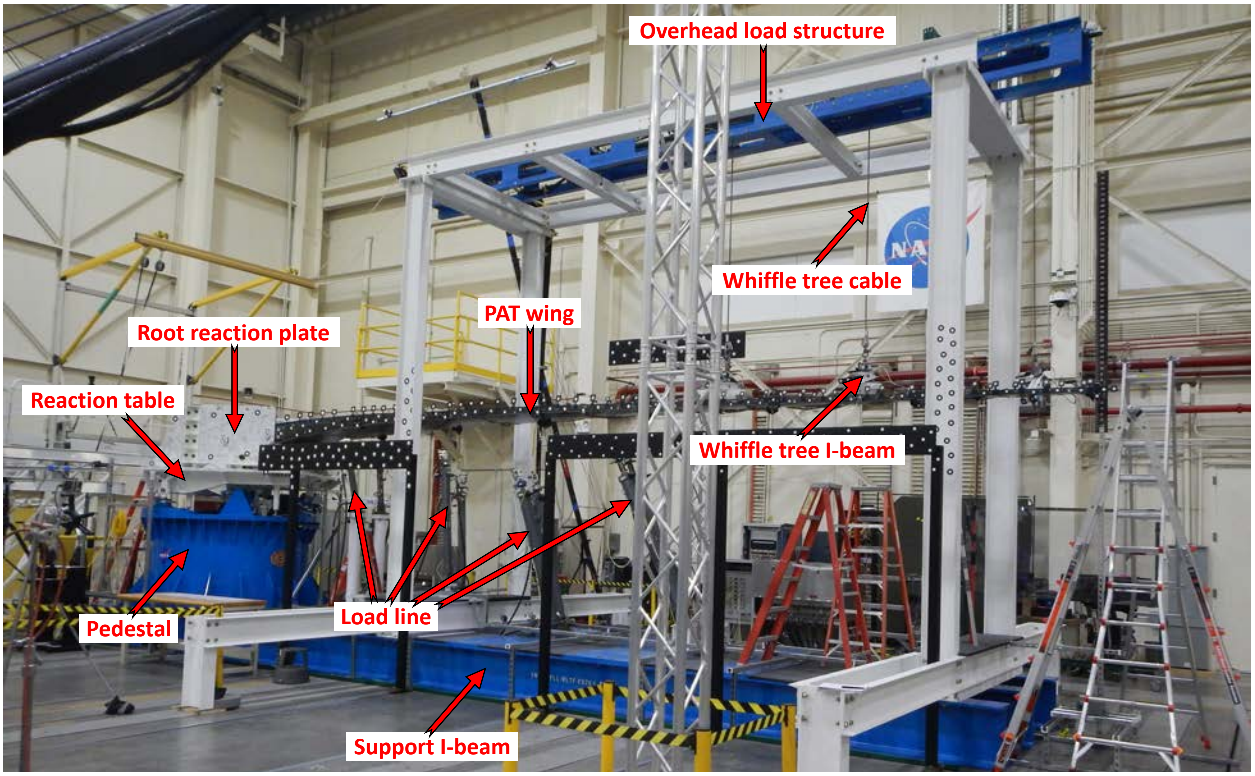

Figure 2. PAT wing test setup.

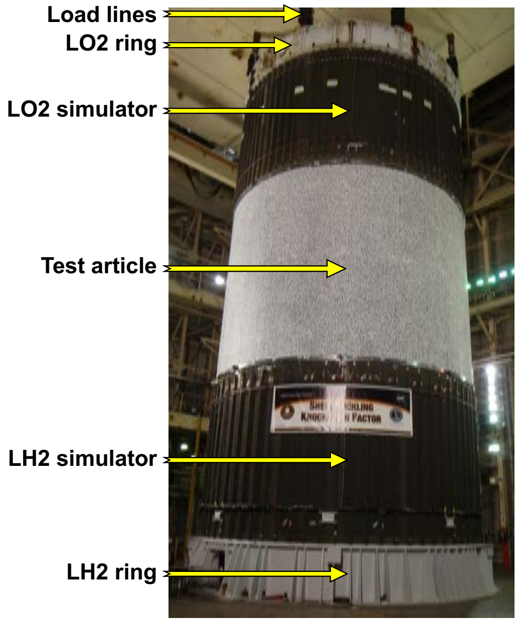

Figure 3. SBKF full-scale metallic barrel test setup.

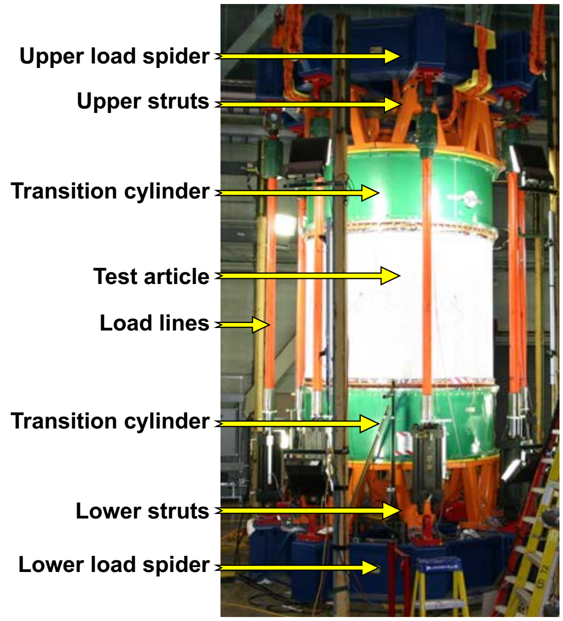

Figure 4. SBKF 8-ft metallic barrel test setup.

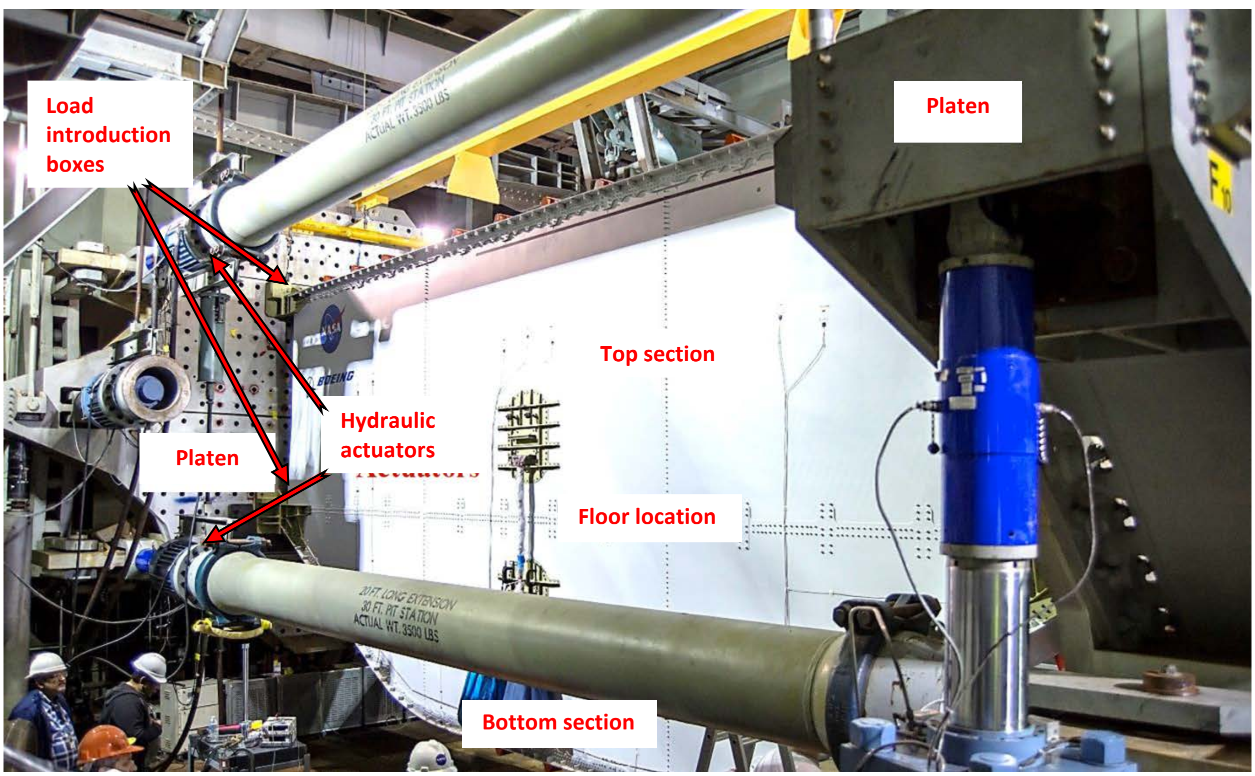

Figure 5. MBB test setup.

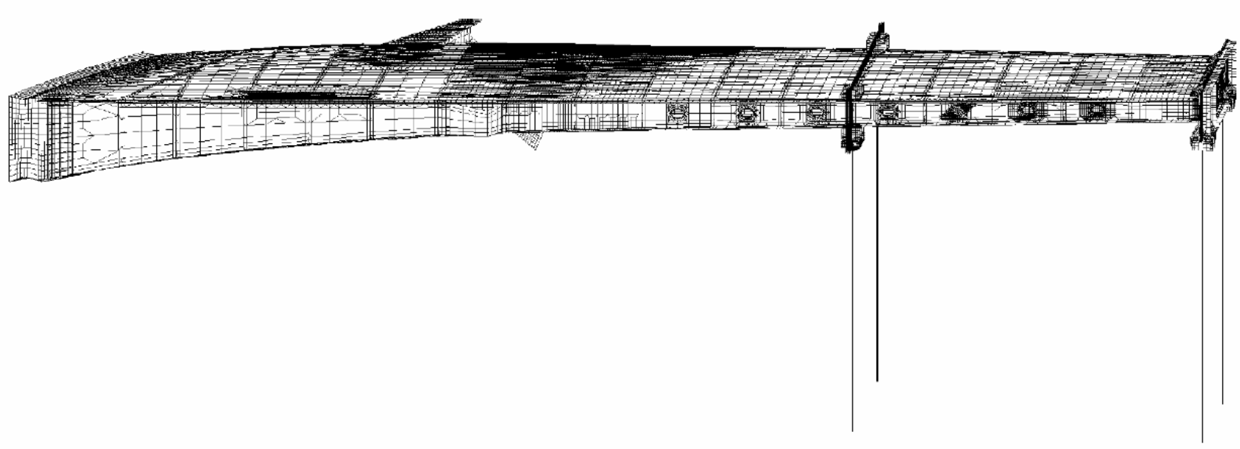

Figure 6. Stitched composite finite element model with outboard load lines and fixturing explicitly modeled. [from Ref. 1]

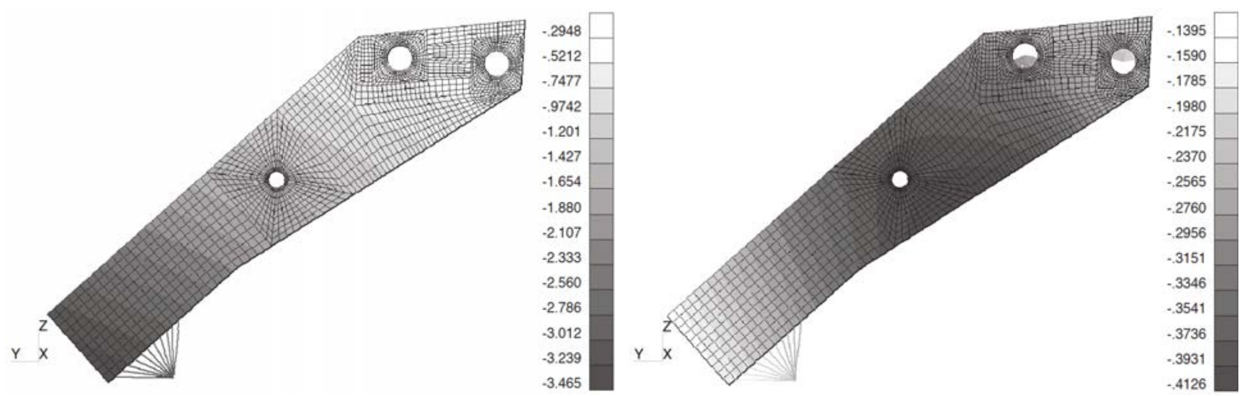

a) Original design **b) With added side-control actuator**

Figure 7. Stitched composite wing braked-roll load arm nonlinear predicted x-deflection (in.) comparison at maximum load. [from Ref. 9]

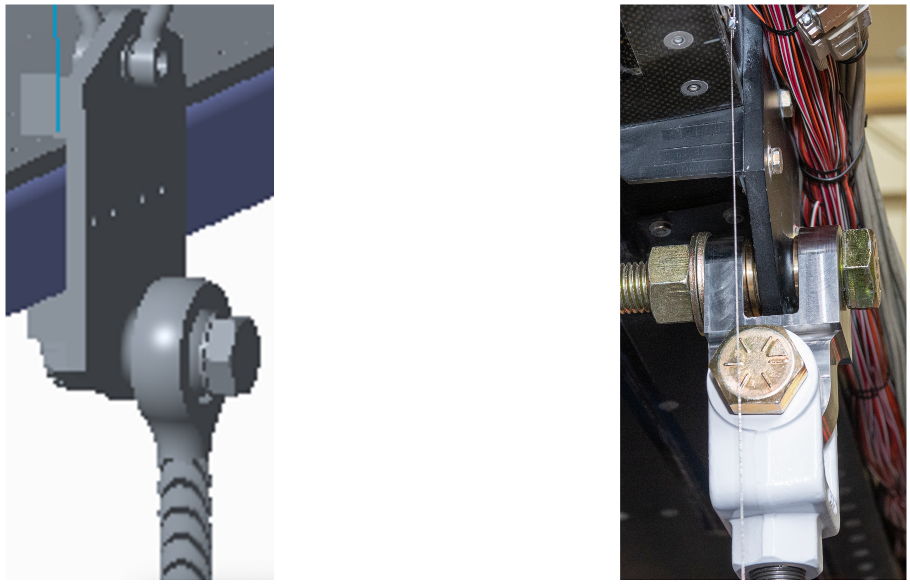

a) Original design

b) Implemented re-design
(from AFRC2018-0091-608)

Figure 8. PAT wing lug load introduction modification to relieve lug stresses.

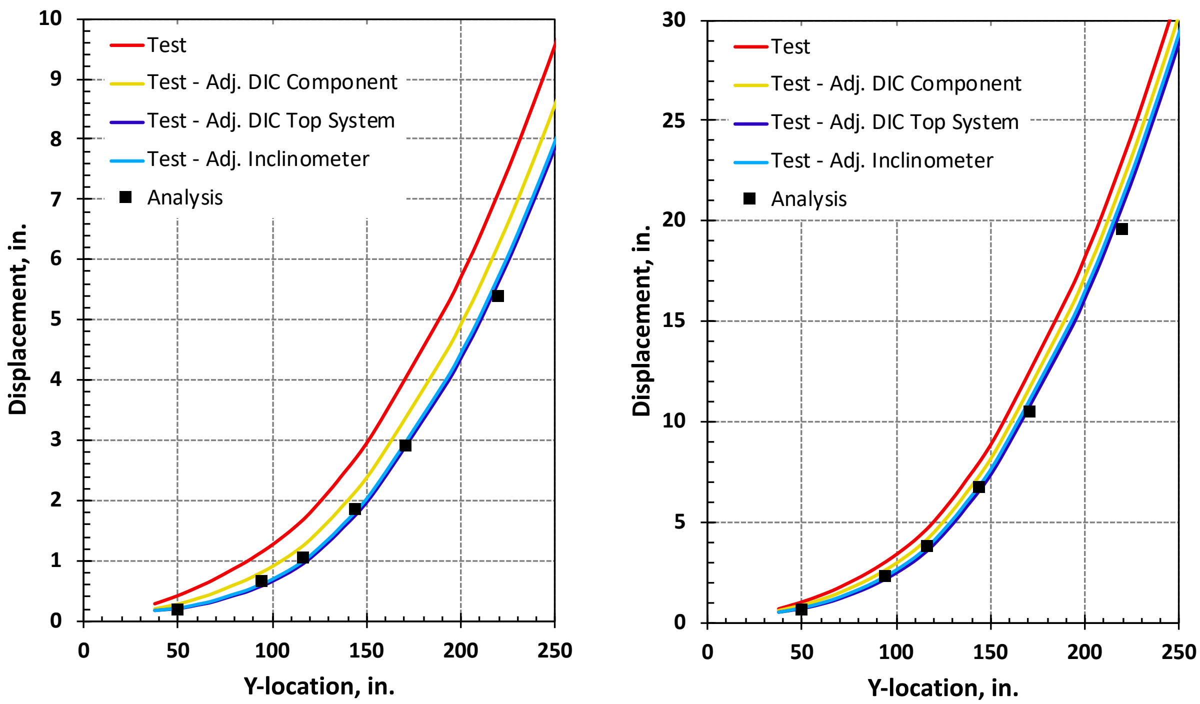

a) At 25% load

b) At 90% load

Figure 9. Inboard trailing edge deflection at 25% and 90% of 2.5g up-bending load. [from Ref. 10]

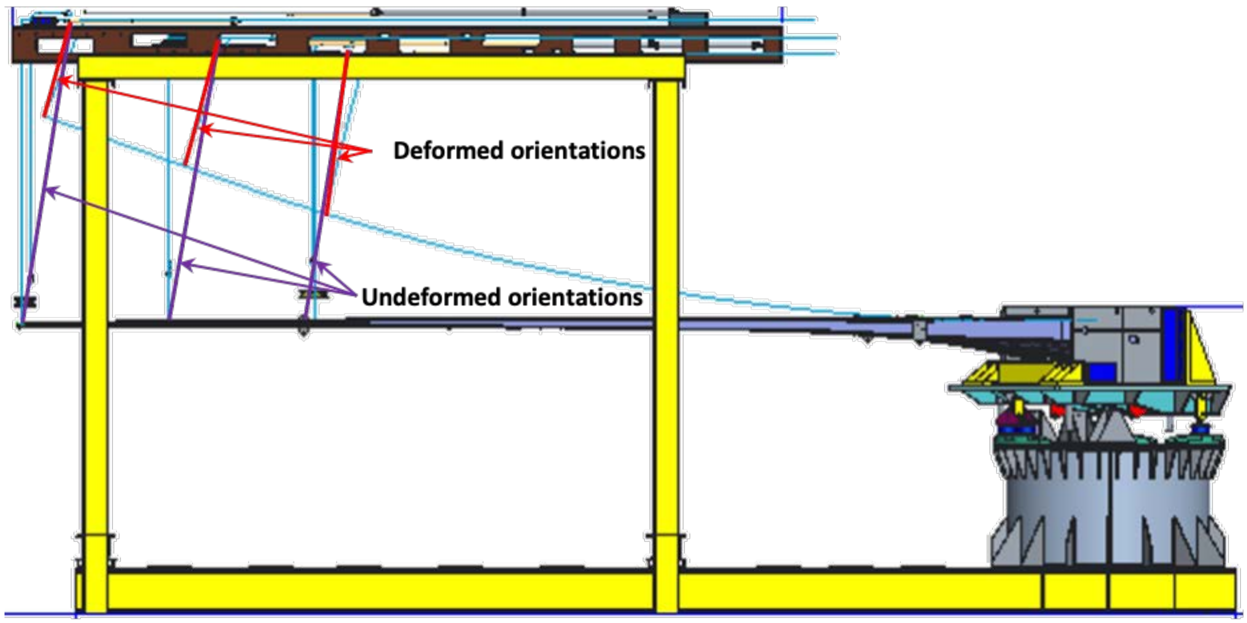

Figure 10. PAT wing upper loading structure cable orientations for undeformed (purple lines) and deformed (red lines) configurations.

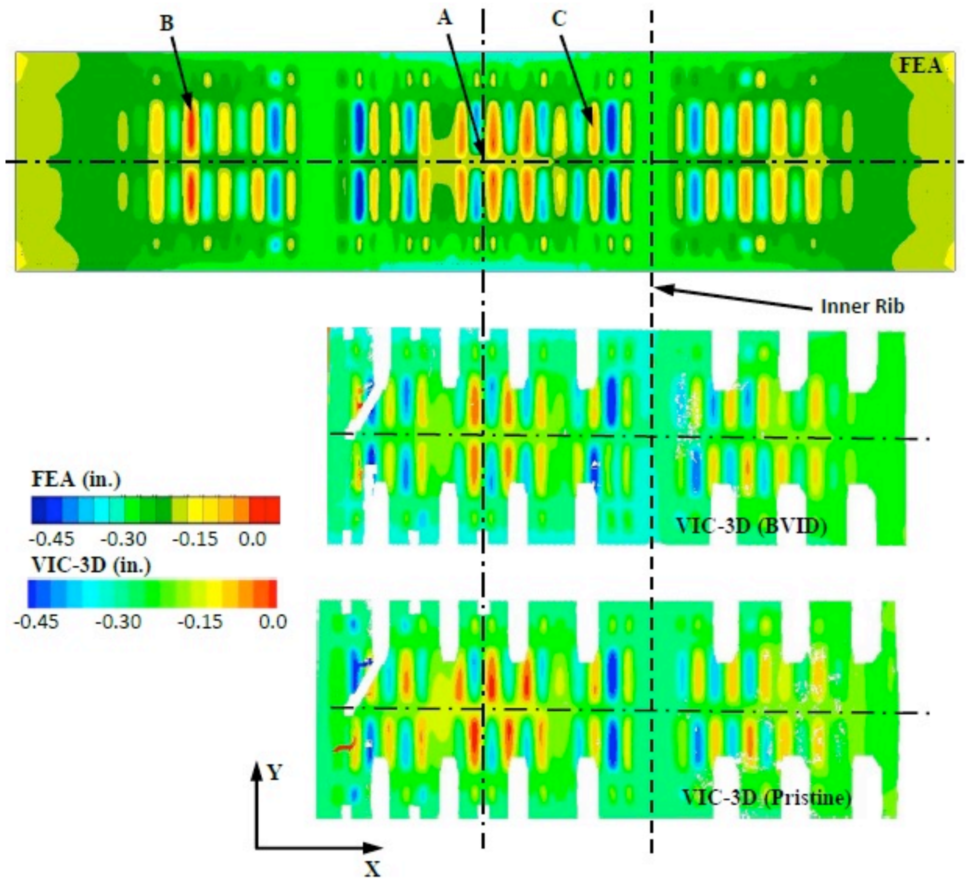

Figure 11. Out-of-plane deformation of the crown panel under 2.5-g DUL. [from Ref. 11]

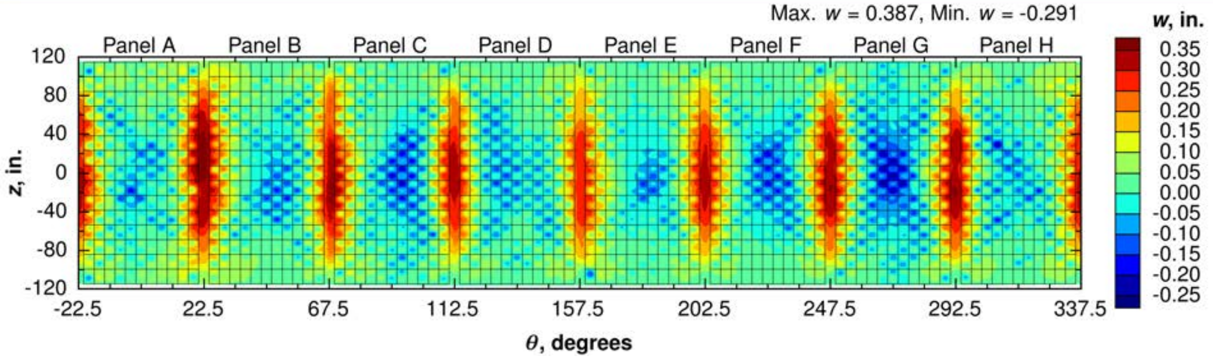

Test

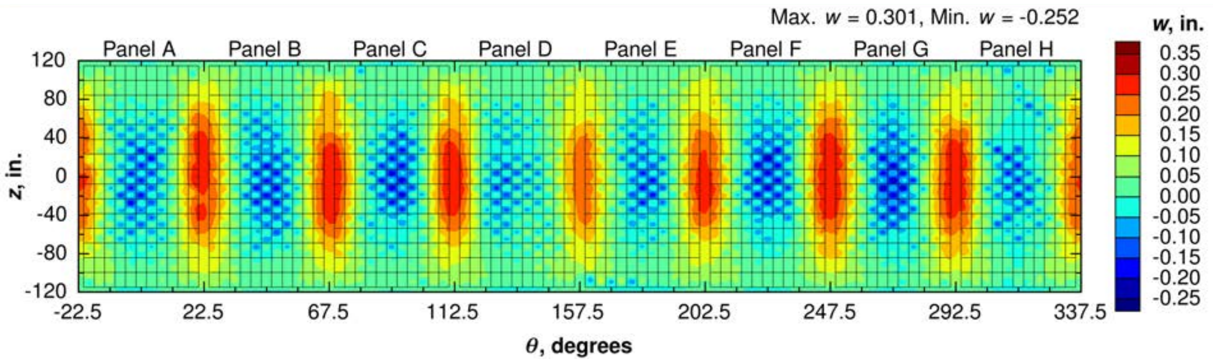

Baseline analysis

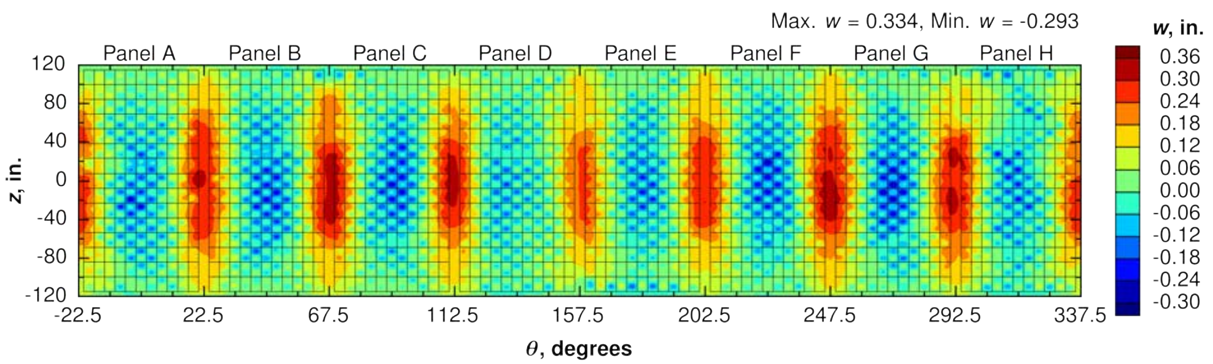

Analysis with residual stresses included

Figure 12. ETTA1 radial displacement (in.) at 1.0 psi and 795 kip axial load. [taken from Ref. 12]